Considering lacustrine erosion records and the De Ploey erosion model in an examination of mountain catchment erosion susceptibility and precipitation reconstruction

Deonie Allen, Anaëlle Simonneau, Gaël Le Roux, Florence Mazier, Laurent Marquer, Didier Galop, Stéphane Binet

▶ **To cite this version:**

Considering lacustrine erosion records and the De Ploey erosion model in an examination of mountain catchment erosion susceptibility and precipitation reconstruction

Deonie Allen [a], Anaëlle Simonneau [b], Gaël Le Roux [a], Florence Mazier [c], Laurent Marquer [a, c, d], Didier Galop [c], Stéphane Binet [a, b]

[a] *EcoLab (Laboratoire Ecologie Fonctionnelle et Environnement), ENSAT, UMR-CNRS 5245, Castanet Tolosan, France*
[b] *ISTO, CNRS UMR 7327, Université d'Orléans, BRGM, France*
[c] *GEODE, UMR-CNRS 5602, Université Toulouse Jean Jaurès, France*
[d] *Research Group for Terrestrial Palaeoclimates, Max Planck Institute for Chemistry, Mainz, Germany*

ARTICLE INFO

ABSTRACT

Reconstruction of paleo-precipitation can provide an insight into past climate and precipitation. De Ploey et al. (1995) presents a highly simplified erosion equation to consider precipitation and erosion susceptibility. This empirical model allows estimation of total precipitation and erosion susceptibility across a range of catchment characteristics (including catchment area, slope, elevation, vegetation cover) and when limited catchment or meteorological data is available. The presented study tests the De Ploey equation using dated lacustrine records of catchment soil deposition both spatially and temporally. The objective is to examine the De Ploey equation's ability and efficiency in reconstructing past long-term precipitation using sedimentological parameters. The erosion susceptibility factor is described as a 'black box' value by De Ploey et al. (1995). This research unravels the erosion susceptibility variable, identifying it to change spatially and temporally according to precipitation, vegetation cover and composition (the extent of tree establishment across the catchment), total lacustrine deposition and geochemical signatures in the archive. Calculation of the erosion sustainability variable and it's use within the De Ploey erosion equation illustrate a reconstruction of an indicative mean annual precipitation and erosion susceptibility change over the recent period (~100 years).

Acronyms and Abbreviations

rAP	Red Amorphous Particles
Rb	Rubidium
Ti	Titanium
Pb	Lead
A	Catchment area (m^2)
P	Precipitation (m)
h	Surface erosion depth (m)
g	Acceleration due to gravity (ms^{-2})
M	Lacustrine total soil and sediment deposition (autochthonous and allochthonous sediment) (per sample)
Ve	soil volume eroded from the contributing catchment (m^3)
Ve(rAP)	volume of rAP represented eroded soil (m^3)
Ve(Rb)	volume of Rb represented eroded soil (m^3)

Es	contributing catchments erosion susceptibility (s^2/m^2)
Es$_L$	published literature erosion susceptibility values (s^2/m^2)
Es$_C$	catchment calculated erosion susceptibility (s^2/m^2) using known erosion, precipitation and catchment area
Es$_C$ (rAP)	catchment calculated erosion susceptibility (s^2/m^2) for rAP represented soil erosion
Es$_C$ (Rb)	catchment calculated erosion susceptibility (s^2/m^2) for Rb represented soil erosion
Es$_D$	catchment erosion susceptibility (s^2/m^2) derived from regression analysis
Es$_D$ (rAP)	catchment erosion susceptibility (s^2/m^2) derived from regression analysis for rAP represented soil erosion
Es$_D$ (Rb)	catchment erosion susceptibility (s^2/m^2) derived from regression analysis for Rb represented soil erosion
S	the quantity of eroded soil in the lake sediment deposition (mg/mg)

Ac	accumulation of total soil and sediment deposition in the lake (m) for respective period
LA	lake area equivalent to the lake deposition extent (m^2)
t	the period represented by the sample (years)
R^2	Coefficient of determination
RMSE	Root mean square error
NSE	Nash-Sutcliffe efficiency
MAE	Mean absolute error
^{10}Be	Beryllium isotope 10
Sr	Strontium
^{137}Cs	Caesium isotope 137
$\delta^{18}O$	Oxygen isotope 18
a.s.l.	above sea level
Sqrt	Square Root
log	Logarithm base 10

1. Introduction

In the global warming context, finding new proxies for the estimation of paleo-temperatures and paleo-precipitation are essential to assess the resilience of terrestrial ecosystems to abrupt changes. However, paleo-precipitation reconstructions that contain long-term trends and extend prior to medieval times are difficult to find and interpret, and depend not only on the time resolution of natural archives but also on the pertinence and the sensibility of both the proxy used and the chosen archive (Seddon et al., 2014). Past precipitation reconstructions can, for example, be based on tree ring records (Buntgen et al., 2011), pedogenetic magnetic susceptibility variations (Maher and Thompson, 1995), cave records (Hu et al. 2008), pollen assemblages (Peyron et al., 1998), glacial dynamics (Holzhauser et al., 2005), lake-levels records (Magny et al., 2011) or flood events deposits (Wilhelm et al., 2012). Precipitation reconstruction is also often completed directly from lacustrine proxy analysis (such as ^{10}Be and $\delta^{18}O$, goethite/hematite ratio, granulometry, ^{10}Be, Sr, Pb, ^{137}Cs, Ti), with short gauged precipitation records available for validation of empirical or numerical precipitation calculations (Cross, 2001; Hyland et al., 2015; Rozanski et al., 1997; Zhou et al., 2014). This constrains the analysis to discussion of 'more' or 'less' humid periods rather than quantifying the amount of past precipitation (Arnaud et al., 2012; Bjune et al., 2005; Magny et al., 2011; Peyron et al., 1998; Simonneau et al., 2013a). Because precipitation, in conjunction with vegetation cover, is a significant driver in erosion processes, soil erosion fluxes stored in lacustrine archives can potentially provide an insightful indication of past trends and overall precipitation (Simonneau, 2012). Past trends in catchment erosion susceptibility reflect both the land use and climatic changes influencing a specific catchment and the sensitivity of that catchment to precipitation driven erosion.

Numerous organic or inorganic parameters can be measured within lacustrine sediments and interpreted as representative of erosion dynamics of the catchment (Arnaud et al., 2016). However, if these sedimentological erosion proxies provide an indication of terrestrial fluxes over time, they do not always assess the nuances of soil-to-sediment differentiation (Arata et al., 2016; Bajard et al., 2017; Charreau et al., 2011; Davies et al., 2015; Ritchie and McHenry, 1990).

The red Amorphous Particles content in a lacustrine archive (rAP, (Chassiot et al., 2018; Foucher et al., 2014; Graz et al., 2010; Simonneau et al., 2014, 2013a)) is one organic sedimentological proxy indicating soil erosion from catchment surfaces to sinks, such as lakes. rAPs are indicators of allochthonous organic catchment soils, e.g. Histosol or Leptosol in a high altitude context (Di-Giovanni et al., 1998; Graz et al., 2010). Lacustrine rAP records provide a quantitative representation of allochthonous soil deposition (Chassiot et al., 2018; Guillemot et al., 2015; Simonneau et al., 2013c, 2013a, 2013b). These

organic particles are approximately 100 μm in diameter and are the result of lingo-cellulosic fragment degradation in soil profiles (Di-Giovanni et al., 1998; Simonneau, 2012).

Minerogenic or inorganic soil representation can be considered through analysis of rubidium (Rb). Rb has classically been used as a tracer of soil erosion in lacustrine archive studies and adopted as a lithogenic soil tracer (Davies et al., 2015; Hosek et al., 2017; Jin et al., 2001; Sabatier et al., 2014; Schmidt et al., 2006; Simonneau et al., 2013a). Combining rAP and lithogenic soil traces can present a more complete and detailed overview of soil erosion dynamics and soil weathering over time (Chassiot et al., 2018; Oliva et al., 2004). The long-term organic and minerogenic fluxes may therefore be used to estimate the amount of precipitation relative to erosion processes.

Modelling such fluxes over long timescales continues to be a challenge as the majority of soil erosion models only function at short timescales (event or pluriannual) and require significant data, such as soil infiltration, roughness or hydraulic conductivity, rainfall event intensity and soil composition. It is acknowledged that the erosive effect of precipitation is dependent on precipitation intensity (especially rainfall intensity) (Lana-Renault et al., 2007; Ziadat and Taimeh, 2013) and, within mountainous catchments, the delineation between snow and rainfall in the precipitation record. However, this level of detail is difficult to establish when using larger timesteps (e.g. 10 years) and lacustrine or paleo archive records. The De Ploey's empirical model of erosion and precipitation is a purposefully simplified method to consider catchment soil erosion across extended time periods (long term) up to and in excess of 100 years (De Ploey et al., 1995). It was designed to approach erosion analysis at a regional or local scale and to consider sediment budgets within a chosen catchment. The De Ploey equation focuses on mean total precipitation as one, quantifiable, driving force behind catchment erosion, without consideration of intensity or snow/rain influence. The second key parameter is the catchment erosion susceptibility (Es), a value selected (but not specifically calculated) by catchment characteristics (location, climate and vegetation, catchment parameters such as slope length and gradient). This model is not well known or frequently used for actual erosion-precipitation modelling due to its lack of complexity regarding soil structure or soil humidity. However, its simplicity may provide a useful method to examine past long-term precipitation, erosion and catchment erosion susceptibility at a decadal time step and over millennia. Es values have been published for of over 60 catchments located globally, using samples that presented time steps of 2 years for some locations (with high deposition rates) to samples with time steps of >500 years. The published range of Es values, relative to generalised catchment conditions for long term erosion susceptibility analysis, generally range from $10^{-3} – 10^{-6}$ s^2/m^2, (De Ploey et al., 1995 and Fig. 1).

To date, the calculation of Es in temporal datasets using multiple samples has not been tested (e.g. lacustrine record). Es could be utilised in one of two ways: firstly, as a coefficient (static value) selected for the catchment due to the general catchment characteristics (e.g. high altitude, temperate climate, general open vegetation); secondly, as a variable that changes over time due to one or a combination of changing meteorological and catchment characteristics and more particularly the vegetation cover.

Identification of catchment soils, through use of quantitative palynofacies soil proxies (Chassiot et al., 2018; Foucher et al., 2014; Graz et al., 2010; Simonneau et al., 2013c, 2013b, 2013a), within lacustrine records provides a temporal erosion record for the study catchments. Using this quantified soil erosion record, this research aims to identify a method to calculate the Es value(s) and present a reconstruction of recent precipitation (~1960-present). To undertake this assessment there are two key assumptions made. First, that the soil proxies used within the lacustrine archives are directly representative of the soil eroded from the contributing catchment and deposited in the lake. Sec-
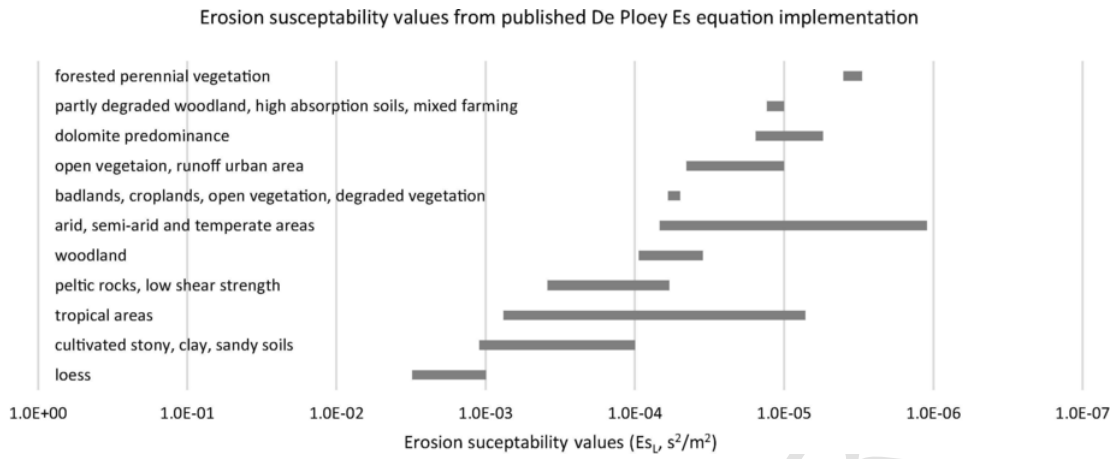
Erosion susceptibility values from published De Ploey Es equation implementation

Fig. 1. Long-term erosion susceptibility values (ES$_L$) from published De Ploey Es equation implementation (reconstruction of catchment characteristics from De Ploey et al., 1995 Figs. 2–4, 6).

ond, that there is negligible loss of eroded material from the lake, that the lacustrine deposition presents a strong catchment soil erosion record (Ouahabi et al., 2016).

2. Materials and methods

2.1. Spatial and temporal lacustrine dataset

Lacustrine records provide dated archives of soil deposition within a lake catchment (Arnaud et al., 2016). For catchments located at the most upstream extent of a larger watershed or basin, these lakes can be the first or primary deposition point for eroded soil. A spatial dataset was created to evaluate the functionality and variability of the De Ploey equation and Es variable across the French Pyrenees and in the French Alps. This dataset is comprised of lacustrine sediment cores from lakes located in the upstream extent of mountain watersheds of varying size, elevation, contributing catchment area, meteorological conditions and vegetation cover. These lacustrine records were used to identify the quantity of eroded soil deposited into the lake: (1) over the last few years (top-core samples, spatial dataset, Fig. 2 and Table 1); and (2) over the last 100 years (looking at the highest resolved lacustrine archive, temporal dataset, Table 2). The spatial dataset was comprised of the most recent 10 mm of sediment deposition from each lacustrine core. The top-core samples present an archive spanning from
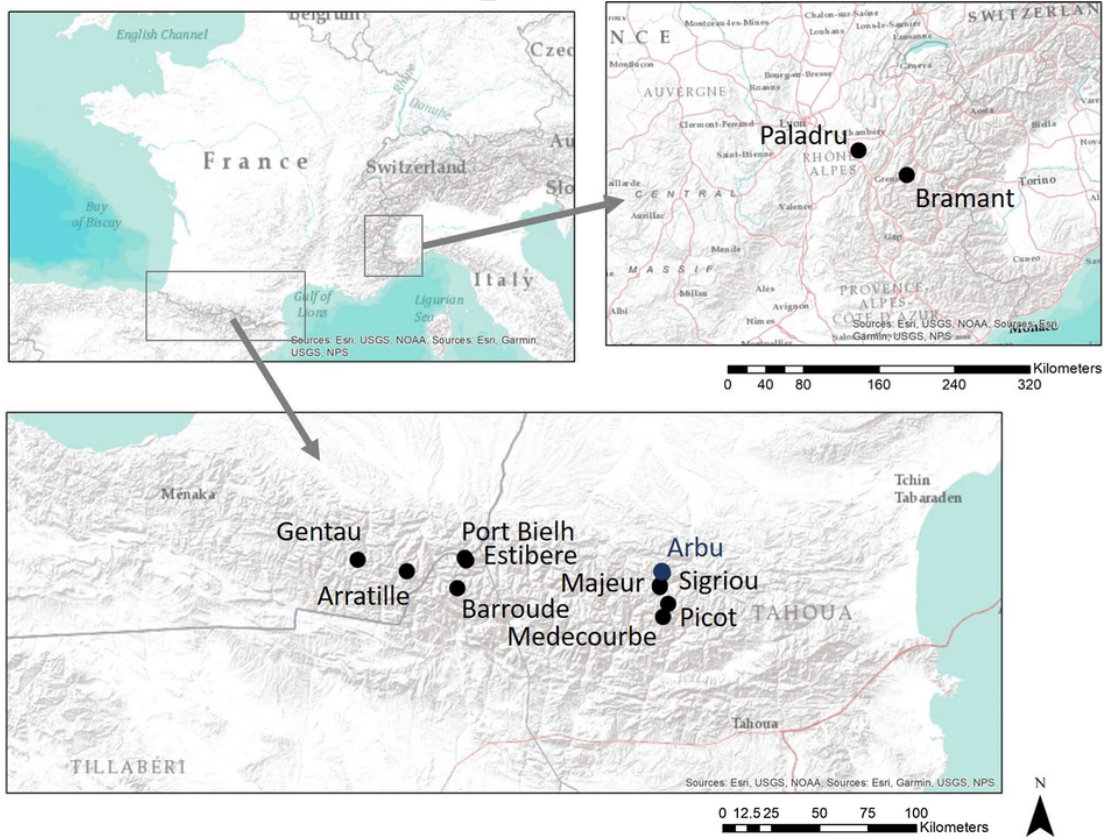

Fig. 2. Study lakes and catchments used in the temporal and spatial analysis of erosion susceptibility. The temporal site, Arbu, is noted on blue. (For interpretation of the references to colour in this figure legend, the reader is referred to the web version of this article.)

Table 1
Dataset of study area lakes and the catchment characteristics.

Catchment and lake name	Location	Catchment area (km²)	Elevation (m a.s.l.)	Lake surface area (km²)	Indicative catchment slope (m/m)	Annual average precipitation (m)	Indicative small tree % vegetation cover	% sparse & natural vegetation cover	% bare rock cover
Arratille	42°47′23″N 0°10′27″W	3.3	2395	0.06	0.20	1.70	4%	34%	66%
Barroude	42°43′52″N 0°8′43″E	1.6	2565	0.11	0.39	1.69	40%	42%	58%
Gentau	42°50′53″N 0°29′14:W	1.9	2023	0.09	0.11	1.78	5%	100%	0%
Majeur	42°5053″N 0°2914″W	9.1	1971	0.21	0.17	1.67	11%	54%	41%
Port Bielh	42°5145″N 0°1036″W	2.0	2440	0.16	0.24	1.47	5%	15%	85%
Sigriou	42°5053″N 0°2914″W	0.4	2168	0.01	1.09	1.58	9%	34%	66%
Paladru*	42°50 53″N 0°2914″W	66.6	1168	3.6	0.01	1.01	16%	17%	0%
Picot	42°40′36″N 1°28′36″E	1.2	2412	0.06	0.24	1.44	23%	25%	75%
Medecourbe	42°5053″N 0°2914″W	1.7	2299	0.04	0.28	1.67	6%	29%	71%
Estibere	42°51′4″N 0°9′37″E	0.4	2425	0.02	0.49	1.51	3%	10%	90%
Bramant*	42°5053″N 0°2914″W	14.7	2658	0.15	0.13	1.43	7%	38%	44%
Arbu	42°48′18″N 1°26′15″E	1.6	1940	0.04	0.39	1.63	26%	100%	0%

Table 2
Sample age (top of sample) and time step durations, element content, deposition of eroded soil (Ve) and erosion susceptibility (Es$_C$, Eq. (1)) (calculated from the original De Ploey Es equation (De Ploey et al., 1995)). * indicates lakes located in the Alps. Indicative deposition volume (M) is calculated following the methods published in (Simonneau, 2012).

	Sample Identification	Sample top date	Sample duration represented (time step) (years)	Ti:Rb	Ti (peak area)	Indicative deposition volume (M) (m³)	Ve(rAP) (relative volume, m³)	Es$_C$(rAP) (s²/m²)	Ve (Rb) (relative volume, m³)	Es$_C$(Rb) (s²/m²)
	Arratille	2013	18	1.80	2408	590	5	5.2E-06	128	1.2E-04
	Barroude	2012	26	2.39	14,995	1122	32	4.5E-05	1015	1.4E-03
	Gentau	2012	50	1.45	8407	868	11	6.5E-06	727	4.3E-04
	Majeur A	2010	14	3.35	1620	2056	157	7.5E-05	200	9.5E-05
	Majeur B	2011	17	17.48	51,072	2056	111	4.3E-05	898	3.5E-04
	Port Bielh	2013	58	1.95	2542	1612	21	1.3E-05	341	2.0E-04
	Sigriou	2012	59	2.02	46,105	132	5	1.4E-05	53	1.5E-04
	Paladru A*	2009	7	1.74	1044	36,048	87	1.8E-05	1454	3.1E-04
	Paladru B*	2009	12	14.11	1044	36,048	87	9.7E-06	1454	1.6E-04
	Picot	2013	17	0.61	1251	611	10	3.2E-05	89	2.9E-04
	Medecourbe	2013	38	1.50	2279	430	7	6.6E-06	79	7.0E-04
	Estibere	2012	172	2.07	1616	165	4	3.8E-06	45	4.3E-05
	Bramant*	2007	26	14.11	45,917	1529	1	2.5E-07	162	1.9E-04
	Arbu	2013	7	4.11	3775	423	7	3.6E-05	67	3.6E-04
temporal dataset	Arbu 1b	2006	8	3.51	4137	423	6	2.7E-05	63	3.0E-04
	Arbu 2b	1998	10	4.25	4397	381	11	3.9E-05	55	2.2 E-04
	Arbu 3b	1988	14	3.97	5350	437	8	2.2E-05	123	3.1 E-04
	Arbu 4b	1974	14	2.74	5679	451	8	2.2E-05	142	4.3 E-04
	Arbu 5b	1960	11	4.57	6101	381	6	2.1E-05	133	4.9 E-04

7 years in sediment and soil deposition record (e.g. Lake Arbu) to > 50 years (e.g. Lakes Sigriou, Port Bielh and Gentau). Lake Arbu, a small alpine catchment in the Mid-Pyrenees with a high lacustrine deposition rate, was adopted for the temporal analysis (analysis of the last 100 years using a 1.15 m high-resolution core; the recent 100yrs is represented by ~70 mm).

Lake cores were collected generally from the central most section of the lake. Cores were recovered from beneath the lake floor using a UWITEC coring device operated from a floating platform or similar (Arnaud et al., 2016; Doyen et al., 2016; Simonneau et al., 2013a).

One core was used from each lake, a common and accepted analytical method in paleorecord analysis (Baddouh et al., 2016; Mügler et al., 2010; Wischnewski et al., 2011), with two cores sampled from Lakes Majeur and Paladru as a methodology check. This spatial dataset encompasses catchments with a range of lake sizes (0.02–3.60 km²), contributing catchment areas (0.37–66.62 km²), altitudes (1168–2658 m a.s.l.), and indicative catchment slopes (0.01–1.1 m/m). The vegetation composition, extent and land use also vary across these catchments, with areas such as Barroude, Gentau, Medecourbe and Sigriou dominated by bare rock, Arbu, Arratille, Picot dominated by

scrubby alpine vegetation and urban development found in the catchment of Lake Paladru.

2.1.1. Study area meteorology and catchment characteristics data

Meteorology and vegetation data for all catchments was gathered from the Météo France® precipitation gauging stations and the CORINE land cover dataset. Météo France® provide both gauged precipitation records from field monitoring sites across France and a gridded network of precipitation records (SAFRAN). Wherever possible a local precipitation gauge was used to quantify the precipitation occurring for each study catchment relative to the sample period (e.g. precipitation for Lake Arbu using the Bernadouze meteorology monitoring station for the top sample (7 year time step) (Gascoin and Fanise, 2018; Meteo France, 2019), with confirmation and gap filling using the SAFRAN dataset (Birman et al., 2017; Quintana-Seguí et al., 2017; Vidal et al., 2010). The total precipitation for each year represented by the sample (e.g. for 2006–2013) was identified from these datasets and summed to provide the De Ploey variable P (P is the total precipitation (m per m^2) for the corresponding period of erosion activity (De Ploey et al., 1995)). Precipitation is presented in Table 1 as an annual average representative of the sample duration (e.g. 2006–2013 for the top Lake Arbu sample) to allow a visual comparison and overview of relative precipitation of the study area catchments.

Land cover was identified using the European Union CORINE program database. CORINE is an EU open source database of environmental information. It includes a database of land cover (using 44 land classifications) at a cartographic scale of 1:100,000 (Bossard et al., 2000; De Roo et al., 2003; Feranec et al., 2007). Using the gridded CORINE dataset and catchment areas, the composition of each catchment was defined (Table 1). Where possible, this land cover characterisation was confirmed using pollen reconstruction analysis (available for the temporal dataset for Lake Arbu and spatially for Lakes Paladru, Majeur and Sigriou (Doyen et al., 2016; Marquer et al., 2019)).

The temporal dataset was created using historically recorded precipitation for the Vicdessos catchment of Lake Arbu and the pollen reconstruction of this catchment's vegetation over the past 100 years. Meteo France precipitation datasets from local monitoring sites (Bernadouze, Foix, Vicdessos, and St Girons) in conjunction with the SAFRAN database were used to define the total precipitation for each sample. Pollen reconstruction of past land cover and vegetation type was completed following the techniques presented in Marquer et al. (2019), and follow the Landscape Reconstruction Algorithm (Sugita, 2007) modelling approach using the full length of lacustrine core. This provided an age dated record of land cover and vegetation occurrence for this catchment. The most recent period was also defined using the CORINE database and compared to the pollen reconstruction results to ensure compatibility between the datasets (pollen reconstruction provided equivalent but more detailed information compared to CORINE database details).

2.1.2. Lacustrine age-dating and elemental analysis

All cores were age-dated following the radiocarbon and ^{210}Pb dating techniques described in (Doyen et al., 2016; Simonneau, 2012; Simonneau et al., 2013b). A minimum of three ^{14}C dates were obtained for each core (bottom, mid and upper core samples) and ^{210}Pb was analysed at ~10 mm intervals along the core. Combining the ^{14}C and ^{210}Pb results an age-date model (CLAM and/or CRS) (Blaauw, 2010; Pawełczyk et al., 2017; Sikorski, 2019) was created for each core from which top sample (for the spatial dataset) and total core samples (for the temporal dataset) ages and time steps were derived (Table 2).

The element composition within each core was quantified using an ITRAX core scanner core scanner (XRF) (or equivalent) at ~1 mm intervals. XRF core scanning is a non-destructive spectrometry method of elemental analysis (Arnaud et al., 2016; Boës et al., 2011; Melquiades

and Appoloni, 2004) that can provide high resolution element concentration data for sediment samples. Due to the high sampling resolution along a lacustrine core, detailed trend and concentration analysis for the period of lacustrine archive can be achieved. For the study area cores, multi-elemental XRF analysis was undertaken, specifically to define the content of Titanium (Ti) and Rubidium (Rb) in each sample (results in parts per million (ppm) or % weight). Values were corrected relative to known soil content. Rb was specifically selected as a minerogenic soil proxy and Ti as a commonly used geochemical soil reference (Boës et al., 2011) to provide an indication of the minerogenic (Rb) and general (Ti) soil content in the lacustrine core. It is acknowledged that the conversion of XRF data into concentration is a crucial step and difficult to achieve with XRF data alone and the available data used in this study may therefore incorporate errors and uncertainties.

2.2. Organic and minerogenic soil proxies

The rAP proxy was selected to represent an organosoil. It predominates the upper horizons of the catchment soil, is often larger in size and less dense compared to Rb, which is a constituent of predominantly clay-silt sized soil minerals (Wang et al., 2008). To quantify rAP, ~10 mm slices of the lacustrine core were prepared and manually analysed using microscopy following published methods (Simonneau, 2012). rAP is highly sensitive to catchment vegetation composition and cover (decreasing as vegetation occurrence decreases), may move easily in minor precipitation events but may also be easily detained within the catchment due to its size and angular shape. This rAP analysis resulted in a count (quantity) of rAP per sample (% organic soil in the sediment; g/g).

Rb was selected to represented lithogenic, mineral soils. Rb may conversely be less easily released (eroded) in minor precipitation events (being retained in the root zones of vegetated areas, potentially buried under or mixed within the organic soil horizons) but be more easily conveyed once entrained in the catchment runoff. There is also a potential, in major precipitation events, for the localised, easily erodible organic soil (rAP) source to be quickly depleted, resulting in major and prolonged precipitation periods presenting a comparably greater Rb representative soil deposition. Similarly, during major precipitation events the Rb content may also become limited as, especially in mountainous catchments where top soil layers such as that represented by Rb may not be infinite.

The differences in composition and transport of these two soil proxies result in the study catchments presenting differing erosion susceptibility values specific to the soil types (organic (rAP) and lithogenic (Rb)). The two complementary proxies have therefore been used as representations of the organic and inorganic catchment soils eroded and transported into the lacustrine records and have been considered (in the De Ploey Es analysis) separately to provide a more detailed analysis of soil erosion in the study catchments.

2.3. Application of the De Ploey model to lacustrine records

2.3.1. Calculation of Es from the precipitation and erosion dataset (Es_C)

The long term De Ploey equation is defined as (De Ploey et al. (1995), Eq. (3)):

$$E_s = \frac{V_e}{A.P.g.h} \tag{1}$$

where Es is the contributing catchments erosion susceptibility (s^2/m^2), Ve is the total soil volume eroded from the contributing catchment (m^3), A is the contributing catchment area (m^2), P is the total precipitation (m per m^2) for the corresponding period of erosion activity, h is

the affected soil thickness (m, accepted as 0.001 m for long term erosion analysis (De Ploey et al., 1995; Simonneau, 2012)) and g is acceleration due to gravity ($\sim$10 m·s^{-2}) (De Ploey et al., 1995; Summer and Walling, 2002).

The De Ploey equation is effective for catchments where derivation of the erosivity measure is difficult (Renard and Freimund, 1994; Wang et al., 2002). It focuses on catchment erosion yield calculated from recorded total precipitation and contributing catchment area, in conjunction with an Es coefficient. The Es coefficient is described by De Ploey et al. (1995) as a 'black box' value due to the limited statistical derivation currently available. Es can simplistically be regarded as a function of the total quantity of eroded soil relative to the total quantity of precipitation on the catchment over a selected period of time.

The De Ploey erosion susceptibility equation (Eq. (1)) was employed across the spatial and temporal datasets in several steps (Fig. 3). First, the erosion susceptibility parameter was calculated using the known precipitation record, soil deposition quantities and catchment area (P, Ve and A in Eq. (1)). These Es values were defined as the De Ploey calculated Es values, Es$_C$. Using Eq. (1) Es$_c$ specific to the study catchment and time period were derived. To calculate the volume of rAP and Rb soil represented in the lacustrine sample the De Ploey definition of soil volume was used, as described in (Simonneau, 2012) and presented in Eq. (2):

$$Ve_t = S_t x (Ac_t xLA) \tag{2}$$

where t = the period represented by the sample (years), S = the percentage of eroded soil relative to the total amount of sediment deposited in the lake, Ac = the accumulation (depth) of total soil and sediment deposition in the lake (m) for respective period (t), and LA = the lake area equivalent to the lake deposition extent (m^2) (Simonneau, 2012). $Ac_t xLA$ result in the total autochthonous and allochthonous deposition volume in the lake, as published in (Simonneau, 2012) and is further represented as M (m^3).

Es$_c$ can be computed if the volume of eroded soil is known (rAP or Rb proxy for the calculations of Ve; Ve(rAP) or Ve(Rb)), the precipitation for the catchment over the period of analysis is known, the assumption of erosion depth (h) for long term erosion calculations is accepted as 0.001 m and the catchment and lake sizes are defined.

2.3.2. Derivation and calibration of Es from lacustrine archive (Es$_D$)

The calculated Es$_C$ values were correlated to catchment characteristics within the temporal and spatial dataset. Correlation analysis was used to highlight which catchment parameters fluctuated in a similar pattern to the changing erosion susceptibility (and lacustrine erosion record). This analysis was used to identify key parameters that may be effective in calculating Es$_C$. Strongly correlated, significant parameters were incorporated into linear regression to find a function that effectively described Es$_C$ and supported P estimation (Fig. 3).
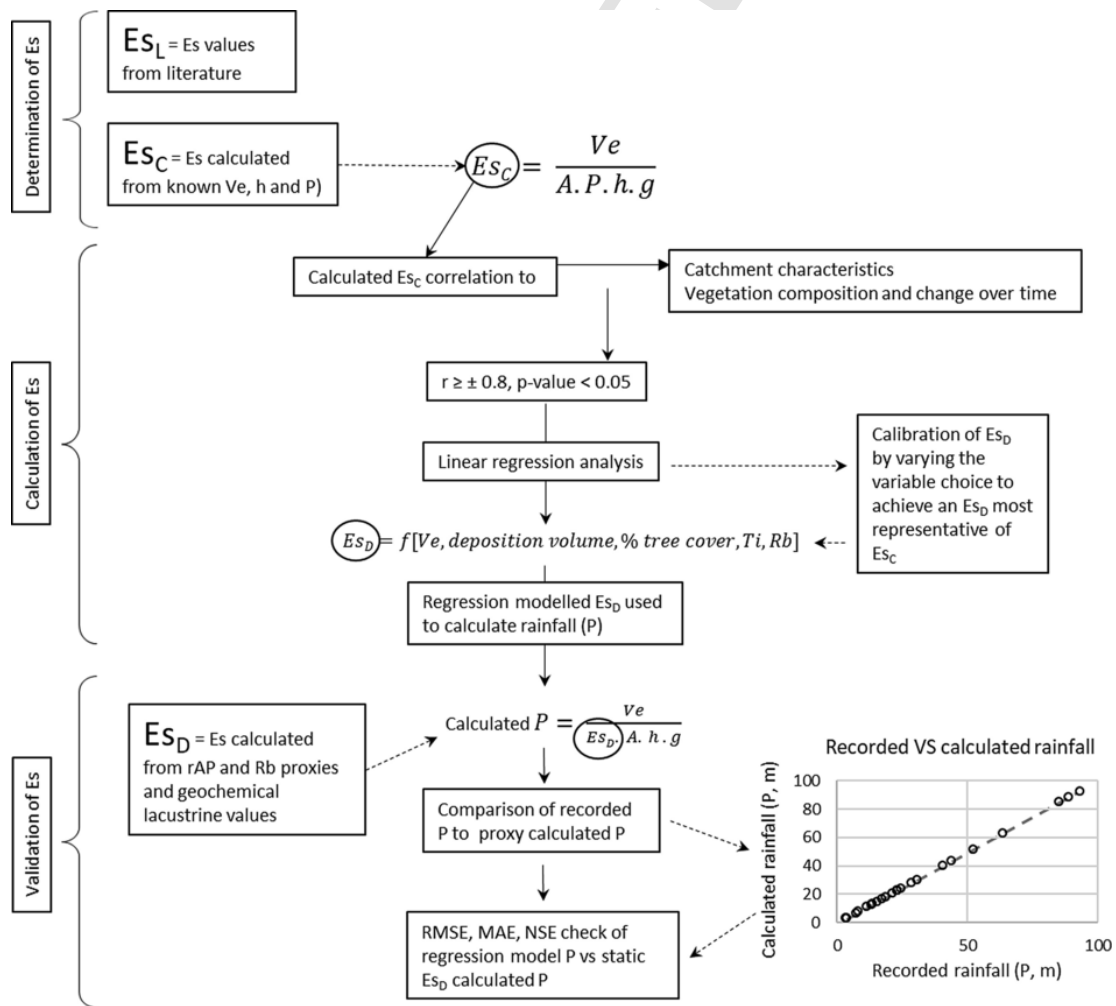

Fig. 3. Schematic of Es and P calculations and analysis.

Using regression analysis, the lacustrine archive datasets (presenting vegetation change, metal, mineral and total deposition over specific time periods) were used to derive a function to reproduce Es_C. These regression Es_C values, defined through archive data, were defined as derived Es values (Es_D). Fig. 3 presents a schematic methodology for the derivation of Es_D.

No single parameter effectively derived Es_C values, necessitating the use of multiple regression analysis. A separate function was defined for $Es_D(rAP)$ and $Es_D(Rb)$ due to the differences in the soil typology and correlation results. The regression analysis was created using the catchment parameters that supported the most effective (strongest coefficient of determination and Nash-Sutcliffe efficiency (NSE)) results.

The multiple linear regression modelling of Es_D was completed using R studio standard functions (lm). Variable selection was made by correlation strength (variables with the strongest and most significant correlation values were selected). The selection of variables used to create the Es_D model were not meteorological parameters, all variables were lacustrine proxy or XRF sampled metal values. This ensured the Es_D model was created from a dataset distinct from the precipitation record, independent from all meteorological data, therefore allowing later validation using recorded precipitation. It was important to define a function with the fewest parameters to support statistical validity in regression function modelling. The number of variables used in the Es_D regression models were kept to a minimum (4) to ensure the number of variables in the equation were less than the number of data points (e.g. recorded precipitation data points).

A spatially diverse dataset was necessary to effectively derive the Es_D linear regression function. The temporal analysis was undertaken on Lake Arbu's lacustrine archive. The temporal and spatial datasets were used to help examine the temporal and spatial robustness of the Es function defined through the regression analysis. To test the efficiency of the correlation, statistical model calculation of Es_D was compared to the De Ploey back-calculated Es_C values.

The linear regression function provides coefficient values (a weighting and scaling factor for each variable) for the model and an intersect value, if an intersect $\neq$ to zero is requested. The selection of variables incorporated into the Es_D regression model were varied until the regression analysis provided Es_D values as close to Es_C as possible.

2.3.3. Validation of the method

The effectiveness of the regression to calculate Es_C has been considered using the coefficient of determination of the Es_D function (r^2), root mean square error (RMSE), and Nash-Sutcliffe efficiency (NSE). Relative error, the difference between recorded and modelled precipitation (m, %) was used to assess the accuracy of the Es_D regression function in replicating the recorded total precipitation dataset alongside RMSE and MAE. NSE is a method to quantitatively assess the efficiency and accuracy of a model (Es_D), mean absolute error (MAE) and RMSE are comparisons on the modelled versus observed datasets to define the error in model results. MAE considers the individual differences (for each lacustrine sample), weighted equally. RMSE functions is a similar way but weights the individual errors relative to their size. RMSE results can therefore illustrate outlier or isolated extreme error result occurrence while MAE provides an average magnitude of error.

The uncertainty in Es_D calculation of P using lacustrine archive data was considered in a similar way. The dataset is comprised of physical sample results (lacustrine records) which hold uncertainty due to analytical quantification methodology (Liu and Gupta, 2007). The lacustrine dataset is dated using ^{14}C and ^{210}Pb and this sample analysis incorporates a temporal uncertainty. Consideration of both sampling (e.g. Ve quantification) and age dating uncertainty has been considered in the Es_D calculation of P.

3. Results

3.1. Es variability and potential drivers

Four Es_C datasets have been created, temporal and spatial Es_C from the rAP soil erosion records (resulting in $Es_C(rAP)$) and temporal and spatial Es_C from the Rb soil erosion records (resulting in $Es_C(Rb)$), and these values have been compared with literature reported Es_L values (Fig. 4). The Es_C values calculated using recorded precipitation and lacustrine erosion records generally fall within the literature recommended range (Es_L) (Fig. 4). The temporal Es_C values illustrate a range almost as great as the spatial dataset, approximately an order of magnitude in range. The calculated Es_C values for the temporal dataset are not static.

$Es_D(rAP)$ illustrated a range between 2.5×10^{-7} – 7.5×10^{-5} (mean = 2.4×10^{-5}) while $Es_D(Rb)$ values range between 4.3×10^{-5} to 1.4×10^{-3} (mean = 3.2×10^{-4}) (Fig. 4). There is an order of magnitude difference in the erosion susceptibility, with rAP illustrating a lower erosion potential than Rb, driven by the recorded lacustrine deposition.

3.2. Correlation analysis

Correlation analysis of catchment characteristics was completed to define key Es_C parameters. Table 3 lists the catchment characteristics considered, the respective correlation values with Es_C and correlation significance. Spatial dataset Es_C illustrated minor correlations with catchment area, elevation, slope, total deposition and Ti. Catchment parameters showing moderate correlation with Es_C included average flow path length, soil type and vegetation coverage.

The temporal Es_C datasets show moderate and generally significant correlation to vegetation composition and coverage. Ti, the geochemical catchment characteristic included in this analysis, illustrated a moderate and significant correlation with and temporal Es_C values. Rb was found to correlate to temporal $Es_C(rAP)$ suggesting a possible link or similar trend in rAP and Rb erosion and deposition in the Arbu catchment.

The representation of vegetation cover, described in Table 3 (and Table 1) as 'indicative small tree % vegetation cover', is derived from the corrected pollen vegetation reconstruction in the temporal datasets. This catchment characteristic correlated with Es_C values, suggesting that the erosion susceptibility in the temporal dataset may follow similar trends and illustrating the known driving influence of vegetation cover and change on erosion (Noël et al., 2001; Rosenmeier et al., 2002).
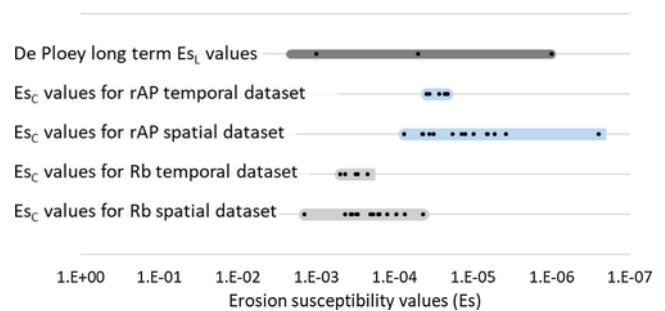

Fig. 4. Es_L value range for long term erosion analysis published in literature (dark grey bar). Es_C values were calculated using the De Ploey equation (Eq. (1)), recorded precipitation and lacustrine erosion records (light grey and blue bars). Dark points within the Es_C ranges illustrate the individual temporal and spatial calculated Es_C values specific to catchment and sample period. (For interpretation of the references to colour in this figure legend, the reader is referred to the web version of this article.)

Table 3
Es$_C$ correlation to geochemical and physical catchment characteristics.

Catchment characteristics	Spatial dataset		Temporal dataset	
	Es$_C$(Rb)	Es$_C$(rAP)	Es$_C$(Rb)	Es$_C$(rAP)
Catchment area (km^2)	−0.17[#]	−0.12		
Lake surface area (km^2)	−0.12	−0.13		
Elevation (m asl)	0.17	−0.09		
Slope (m/m)	0.16	0.13[#]		
Average flow path length (m)	−0.21[#]	0.21[#]		
Soil type	−0.47*	−0.11		
% bare rock	0.03[#]	−0.11		
% sparse vegetation	0.24[#]	0.40[#]		
% small tree vegetation [*]	0.71*	0.51 [#]*	0.67[#],*,*	−0.67*,*
Total deposition (M)	−0.12	−0.13	0.68*	−0.38*
Ti	0.16[#]	−0.01	−0.81*	−0.59 [#],*
Rb	NA	−0.1	NA	0.42[#]
Ti/Rb	NA	0.07[#]	NA	−0.68 [#],*

* = p-value < 0.1.
[*] Vegetation that has been corrected by pollen analysis includes the Temporal dataset and Lakes Paladru, Majeur and Sigriou. Rb and the Ti:Rb ratio have not been included in the assessment of Es$_D$(Rb) and are therefore presented with NA in the table.
[#] Indicates the Log10 transformation of the data.

3.3. Es regression analysis

The Es$_D$(rAP) regression function is derived from the lacustrine erosion record (Ve(rAP)), the total sediment deposition volume (M, m^3) for respective period, the corrected pollen reconstruction model of vegetation pattern (represented as a % of tree cover), and the Ti:Rb ratio (indicator of general erosion and precipitation). It is noted that the Rb:Ti ratio illustrated a stronger correlation to Es$_C$(rAP) however when considered within the multiple regression analysis the inverse ratio (Ti:Rb) presents a model with a more effective coefficient of determination and smaller p-values. The Ti:Rb parameter was therefore included in the regression function.

$$Es_D(rAP) = a.Ve(rAP) + b.M + c.\%tree\ cover + d.Ti : Rb \quad (3)$$

The Es$_D$(Rb) regression is derived from the lacustrine erosion record (Ve(Rb)), the deposition volume (m^3), pollen reconstruction of vegetation patterns (represented as a % of tree cover), and the Ti trend (indicator of general erosion and precipitation).

$$Es_D(Rb) = a.Ve(Rb) + b.M + c.\%treecover + e.Ti \quad (4)$$

The regression coefficients for Eqs. (3) and (4) are presented in Table 4. The coefficients for the temporal, spatial and total (cumulative) datasets of rAP and Rb have been calculated.

The functions presented in Eqs. (3) and (4) have been calculated for the spatial and temporal datasets separately. A 'total dataset' analysis

was completed but while the coefficients defined using the total dataset are relatively effective in modelling Es$_C$, it was noted that separating the temporal and spatial dataset presented greater accuracy in Es$_D$ calculations. For the purposes of this analysis, the spatial and temporal datasets were treated separately to try and define the most effective model possible for the reconstruction of total precipitation for the spatial and temporal datasets. The Es$_C$ values relative to the regression Es$_D$ values are presented in Fig. 5.

The Es$_D$(rAP) values from the regression derivation have a coefficient of determination (r^2) of 0.93 (RMSE of 4.8×10^{-6}) and NSE of 0.93 (Fig. 5a). The Es$_D$(Rb) values from the regression derivation have a coefficient of determination (r^2) of 0.92 (RMSE of 8.3×10^{-5}) and NSE of 0.91 (Fig. 5b). The Es$_D$ regression equations (Eqs. (3) and (4)) illustrate a strong coefficient of determination (r^2 > 0.8) and NSE (0.7 < NSE > 1) suggesting model efficiency in synthesising Es$_C$ values from lacustrine data.

3.4. Estimation of total P using lacustrine record

The total precipitation calculated using Es$_D$(rAP) and Es$_D$(Rb) were compared to recorded precipitation based on a split sample method. Fig. 6 illustrates the modelled P relative to recorded values, and the general trend in P when historic lacustrine data is considered back past recorded P. Both rAP and Rb results illustrate notable uncertainties and errors, however there is some capacity for these Es$_D$ equations to estimate P and provide information on the trends in recent and past P. As a first step towards using a highly simplified, limited data availability model to consider mean annual P, this method could be useful.

The RMSE for the recorded vs modelled P using the rAP dataset and Es$_D$(rAP) equation was 0.29 (total dataset), with the spatial dataset presenting a RSME of 0.32 and temporal dataset RSME of 0.22. The mean absolute error (MSE) for the total dataset was 0.24, 0.22 for the temporal dataset and 0.25 for the spatial dataset. The RMSE and MAE for P estimated using the rAP dataset were <35% of the recorded average annual precipitation. The RSME is higher than MAE for the total dataset and spatial subset, suggesting some extreme results or outliers in the spatial modelled dataset.

The RMSE for the recorded vs modelled P using the Rb dataset and Es$_D$(Rb) equation was 0.34 (total dataset), with the spatial dataset presenting a RSME of 0.40 and temporal dataset RSME of 0.14. The MSE for the total dataset was 0.25, 0.10 for the temporal dataset and 0.32 for the spatial dataset. As with the rAP dataset, the RMSE and MAE (total dataset) are <35% of the recorded average annual precipitation, suggesting no significant difference between the rAP and Rb modelled P results when the total dataset is considered. The RSME is slightly higher than MAE for all Rb estimated P results, suggesting outliers and extreme results across the dataset results. Both modelled P results illustrate a smaller RMSE and MAE for the temporal datasets compared to the spatial datasets, suggesting that using this method is slightly more effective for temporal analysis than when used for the spatial dataset.

The uncertainty in precipitation estimation has been calculated with consideration of the uncertainty in quantifying rAP and Rb (and
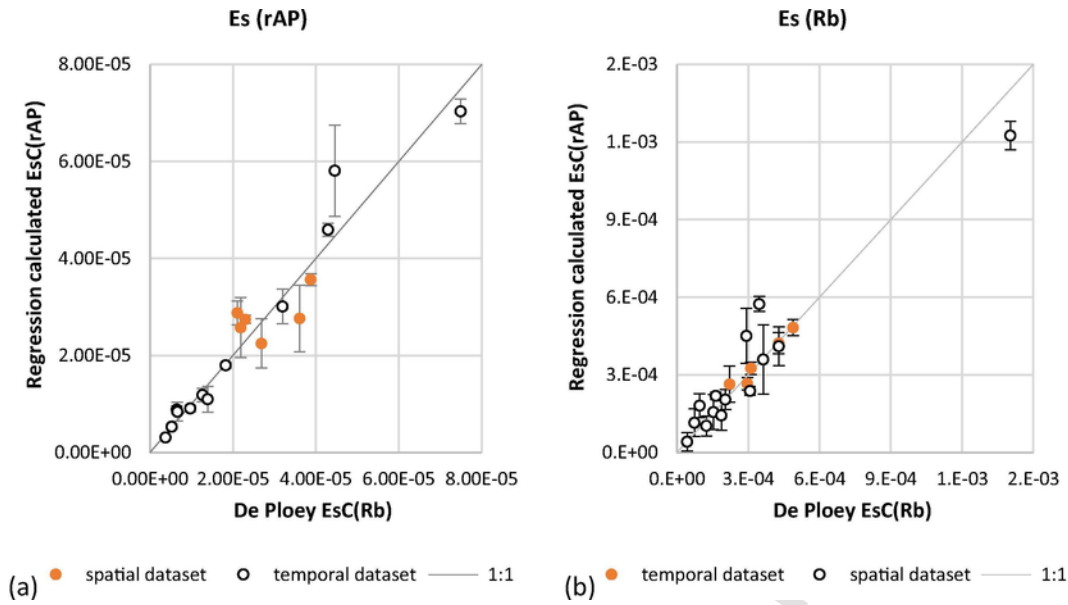
Table 4
Regression analysis coefficients. The regression R^2 are relative to the dataset used in the model, not the total dataset.

	Regression dataset	Intercept	Ve	Total deposition (M)	% tree cover	Ti:Rb	Ti	R Squared	Adjusted R Squared
			a	B	c	d	e		
rAP	spatial dataset	0	4.1E-07	−9.8E-10	1.2E-04	−6.3E-07	NA	0.99	0.87
	temporal dataset	0	2.2E-06	−1.5E-08	2.9E-05	2.9E-06	NA	0.96	0.40
Rb	spatial dataset	0	5.0E-07	−2.1E-08	1.9E-03	NA	−8.1E-06[#]	0.84	0.70
	temporal dataset	0	8.1E-07	2.1E-07	1.4E-03	NA	−3.8E-08	0.99	0.49

[#] Indicates the Log transformed datasets.

Fig. 5. Graphical representation of EsD values calculated using Eqs. (3) and (4) respectively. The spatial dataset Es_D values are illustrated in black outlined points; temporal Es_D values are presented as orange points. The error bars represent the uncertainty range around Es_D calculations when Ve and P values are modified to represent the Ve quantification and sample date uncertainties. (For interpretation of the references to colour in this figure legend, the reader is referred to the web version of this article.)
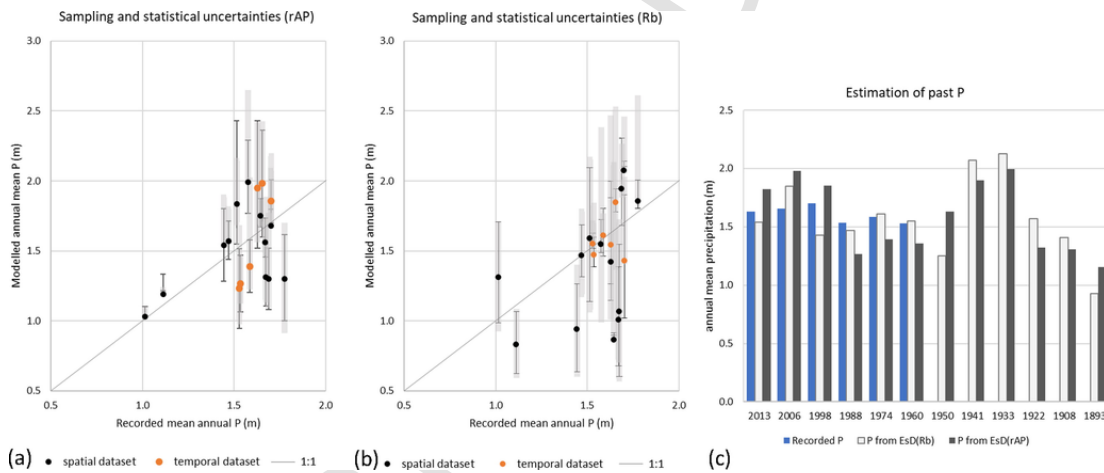

Fig. 6. Calculation of P from regression Es_D(rAP) (6a) and Es_D(Rb) (6b) defined values. The black error bars show the uncertainty in P values due to Ve quantification uncertainty. The grey error bars illustrate the uncertainty in P due to the sample date uncertainty. Spatial P results are presented as black points, Lake Arbu catchments temporal dataset results are presented as orange points. Fig. 6(c) shows the temporal estimated P using historic data extending past the recorded records for Lake Arbu. (For interpretation of the references to colour in this figure legend, the reader is referred to the web version of this article.)

therefore Ve) in the lacustrine archive and the uncertainty in dating the samples. Uncertainty analysis has been completed considering these uncertainty elements individually and cumulatively. The individual (Ve and sample dating) uncertainties are presented in Fig. 5, with the spatial and temporal breakdown of uncertainties is summarised in Table 5.

It is noted that while Es_D was effectively calculated using Eqs. (3) and (4), the calculation of P is highly sensitive to small inaccuracies in Es values, resulting in sizable relative errors in precipitation estimations. A 1% change in Es_D values (without any further uncertainty considerations) results in a relative error in P of −43% to 59% (Rb) and −16% to 34% (rAP). A 1% error or uncertainty in Es values illustrates a similar precipitation calculation error to the Es_D model relative error or uncertainty in Ve quantity.

4. Discussion

4.1. Variable erosion susceptibility (Es)

Literature Es values (Es_L) for long term erosion analysis fall between 1×10^{-3} – 1×10^{-6} s^2/m^2. Es_L values have previously been considered and used as a constant, with little available information on the derivation of the long-term erosion sustainability values. For the first time, lacustrine records of erosion (rAP and Rb indicators of erosion in mountain catchments) have been coupled with catchment specific precipitation records to calculate Es_D values. The simple Es_c calculation illustrates a range of Es_c values falling within the range of published (Es_L) values, but that the definition of Es is difficult unless precipitation and erosion are quantified for the study catchment and respective time period. This makes section of an Es value for use in the De Ploey erosion equation or as a description of a catchment's erosion

Table 5
Summary of uncertainty influence on error.

	dataset		Relative Error (recorded P – modelled P)*		rAP or Rb sampling uncertainty (modelled – uncertainty calculated)*		Age depth uncertainty (modelled – uncertainty calculated)*		sampling + age depth uncertainty (modelled – uncertainty calculated)*	
			max	min	max	min	Max	min	max	min
rAP	Temporal	value	0.30	−0.33	0.35	−0.32	0.73	−0.34	0.48	−1.36
		% change	19%	−20%	23%	−19%	44%	−21%	30%	−87%
	Spatial	value	0.48	−0.42	0.43	−0.49	0.68	−0.58	1.81	−6.07
		% change	−27%	26%	24%	−32%	42%	−32%	28%	−331%
Rb	Temporal	value	0.19	−0.27	0.23	−0.43	0.81	−1.96	0.81	−0.81
		% change	16%	−12%	14%	−26%	49%	−117%	49%	−114%
	Spatial	value	0.78	−0.37	0.76	−0.52	1.55	−2.62	1.56	−5.27
		% change	47%	−29%	45%	−32%	72%	−144%	72%	−305%

* Precipitation values are in metres.

susceptibility challenging, with current selection guidance focused on catchment vegetation and soil typology.

The Es_c value is found to range (for the study catchments) from $1 \times 10^{-3} – 1 \times 10^{-6}$ s^2/m^2 spatially but also temporally. This illustrates that Es_c is not a coefficient but that to achieve effective erosion, erosion susceptibility and precipitation representation using the De Ploey erosion equation over a time period (with multiple sub-samples) the Es value is a variable (as illustrated in Figs. 4 and 5). This is logical, as erosion is driven by vegetation and precipitation, both naturally and anthropically influenced and changing over time. Therefore, given that vegetation and precipitation fluctuate over time, it is important that erosion susceptibility act as a variable which responds to precipitation and vegetation trends, a spatio-temporal variable.

Es_c is noted to correlate most strongly to meteorological conditions. However, if: (1) Es is to be calculated for catchments or time periods where meteorological records are scarce; or (2) the De Ploey equation is to be used to assess historic erosion and precipitation patterns, then Es must be described as a function of non-meteorological parameters. The correlation and simple linear regressions present a description of erosion susceptibility (Es_D) specific to the time period and individual catchment characteristics. This function (Eqs. (3) and (4)) provides a new method to estimate Es for a catchment beyond the use of generalised vegetation and soil descriptions (Es_L). This descriptive Es_D function supports estimation of the temporal and spatial variability in Es based on catchment specific lacustrine erosion and geochemical indicators. The functions are a step towards greater description and understanding of the driving forces and catchment (temporal and spatial) representation of erosion susceptibility.

The difference in lacustrine quantities of rAP and Rb may be due to the relatively thin soil profile in the study (mountain) catchments, organic carbon content in Pyrenees mountain catchments of ~10% (Garcia-Pausas et al., 2007) and correspondingly relatively small quantity of organic soil available for erosion. As a result, there is a smaller quantity of organic soil (rAP) available in the catchment and therefore a correspondingly smaller quantity of rAP in the lacustrine archive. The difference in Es_C values suggests that the erosion susceptibility value may be specific to soil typology and catchment soil availability.

4.2. Lacustrine erosion indicators

The two erosion indicators (rAP and Rb) considered in this study represent different soil types (organo-mineral and mineral soils). Both Es_D functions show effective model capability (0.7 < NSE > 1) how-

ever the effectiveness in precipitation representation using these modelled Es values varies (Fig. 5, Table 5). This is due to the driving influence of the Es parameter in the De Ploey erosion equation, and the resultant sensitivity in calculated precipitation to small changes in Es. It is also due to the coarse reconstruction of precipitation driven erosion possible using the De Ploey method given the lack of differentiation between rainfall and snow in the dataset and the significantly different erosion impact snow and rainfall have on a catchment or soil.

There is limited diference in the representation of erosion susceptibility and precipitation from the two datasets, rAP and Rb. There is slightly greater error and uncertainty in the Rb dataset results compared to rAP. This may be due to the different physical transport properties of these two erosion indicators. rAP are particles that may be broken but do not dissolve or transform. Rb is a property of the underlying (granite) bedrock and soil. Rb absorbance is strongest to fine (silt-clay size) particles (De Vos et al., 2006; Salminen et al., 2015). The Es_D(Rb) function may need an additional parameter (variable) that describes the changing catchment pH, individual precipitation events and soil composition properties (as indicators of the Rb transport mechanisms relative to the time period) to support more effective future Es_D(Rb) modelling.

There is uncertainty in both erosion quantification (sampling) and the age dating model. The rAP and Rb erosion datasets react similarly to these uncertainties. Both datasets illustrate a greater sensitivity to age depth model uncertainty than rAP or Rb sampling uncertainty (Table 5). Both rAP and Rb temporal results show lower sensitivity to sampling and age depth uncertainty than the spatial datasets. This suggests that the Es_D may be more effective for site specific longitudinal (archive) analysis that spatial analysis.

4.3. Snow/rain influence on erosion and De Ploey estimation of past precipitation

A significant proportion of precipitation in mountainous catchments occurs as snow rather than rainfall. Snowmelt may or may not mimic erosion events occurring due to rainfall or be represented clearly in annual precipitation records. Within the lacustrine deposition it is difficult to differentiate erosion due to snow versus rain. Correspondingly, the generalised precipitation available and used in this De Ploey analysis provides no distinction between snow and rainfall precipitation but instead presents an overall precipitation value. As such, the influence of snowfall on these catchments is not taken into account in either precipitation estimation or erosion calculations. This is expected to be a

key influence in the error in De Ploey Es estimation of precipitation using lacustrine records, resulting in inexact estimation of past precipitation as illustrated in Fig. 6.

Furthermore, the influence of rainfall intensity is not taken into account in this De Ploey analysis (total or annual precipitation are the only parameters prescribed, De Ploey et al., 1995). Rainfall intensity is a significant driver of erosion, in conjunction with top soil composition. While the complexities of top soil composition and details of rainfall event intensity are key to erosion, the De Ploey Es model is designed for a gross estimation of precipitation and erosion without provision of intensity or catchment soil complexity. This is therefore a further source or error and uncertainty in the De Ploey estimation of past precipitation.

5. Conclusions

Lacustrine erosion records have been used within the De Ploey erosion equation to consider the erosion susceptibility and precipitation of 12 French mountain catchments. Using recorded precipitation and erosion, the Es_C value for each time step and catchment has been calculated, illustrating Es_C values for these catchments to fall within the published literature. Es_C (and Es_D) values are only representative of the sampled time period analysed and incorporate consideration of the continuously changing climate (precipitation) and vegetation (type and extent) in the specific study area under review. As climate and vegetation change over time, so Es_C values can be expected to change. Results demonstrate that there is complexity in estimating Es_C and that Es_C is a variable when considered in a spatial and temporal context.

Through analysis of the lacustrine archive, a description of the Es_C variable has been created allowing Es_D to be calculated using lacustrine archive data. This supports erosion susceptibility and precipitation estimation for catchments and time periods where either erosion susceptibility or precipitation records are unavailable. While Es_D is effectively calculated, the simulation of P is indicative but inexact, and this analysis illustrates the need for further development of the Es model to accurately reconstruct P using lacustrine records. This research therefore presents a step towards an effective simplistic approach in precipitation reconstruction using lacustrine records and provides a method to define Es values using non-meteorological parameters commonly available for catchments.

Acknowledgements

References

Arata, L., Meusburger, K., Frenkel, E., Campo-Neuen, A.A., Iurian, A., Ketterer, M.E., Mabit, L., Alewell, C., 2016. Modelling Deposition and Erosion rates with RadioNuclides (MODERN) – Part 1: a new conversion model to derive soil redistribution rates from inventories of fallout radionuclides. J. Environ. Radioact. 162–163, 45–55. https://doi.org/10.1016/j.jenvrad.2016.05.008.

Arnaud, F., Poulenard, J., Giguet-covex, C., Wilhelm, B., Revillon, S., Jenny, P., Revel, M., Enters, D., Bajard, M., Fouinat, L., Doyen, E., Simonneau, A., Pignol, C., Chapron,

E., Vanniere, B., Sabatier, P., 2016. Erosion under climate and human pressures: an alpine lake sediment perspective. Quat. Sci. Rev. 152, 1–18. https://doi.org/10.1016/j.quascirev.2016.09.018.

Arnaud, F., Révillon, S., Debret, M., Revel, M., Chapron, E., Jacob, J., Giguet-Covex, C., Poulenard, J., Magny, M., 2012. Lake Bourget regional erosion patterns reconstruction reveals Holocene NW European Alps soil evolution and paleohydrology. Quat. Sci. Rev. 51, 81–92. https://doi.org/10.1016/j.quascirev.2012.07.025.

Baddouh, M., Meyers, S.R., Carroll, A.R., Beard, B.L., Johnson, C.M., 2016. Lacustrine 87Sr/86Sr as a tracer to reconstruct Milankovitch forcing of the Eocene hydrologic cycle. Earth Planet. Sci. Lett. 448, 62–68. https://doi.org/10.1016/j.epsl.2016.05.007.

Bajard, M., Poulenard, J., Sabatier, P., Etienne, D., Ficetola, F., Chen, W., Gielly, L., Taberlet, P., Develle, A.-L., Rey, P.-J., Moulin, B., de Beaulieu, J.-L., Arnaud, F., 2017. Long-term changes in alpine pedogenetic processes: effect of millennial agro-pastoralism activities (French-Italian Alps). Geoderma 306, 217–236. https://doi.org/10.1016/j.geoderma.2017.07.005.

Birman, C., Karbou, F., Mahfouf, J.-F., Lafaysse, M., Durand, Y., Giraud, G., Mérindol, L., Hermozo, L., 2017. Precipitation analysis over the french alps using a variational approach and study of potential added value of ground-based radar observations. J. Hydrometeorol. 18, 1425–1451. https://doi.org/10.1175/jhm-d-16-0144.1.

Bjune, A.E., Bakke, J., Nesje, A., Birks, H.J.B., 2005. Holocene mean July temperature and winter precipitation in western Norway inferred from palynological and glaciological lake-sediment proxies. The Holocene 15, 177–189.

Blaauw, M., 2010. Methods and code for "classical" age-modelling of radiocarbon sequences. Quat. Geochronol. 5, 512–518. https://doi.org/10.1016/j.quageo.2010.01.002.

Boës, X., Rydberg, J., Martinez-Cortizas, A., Bindler, R., Renberg, I., 2011. Evaluation of conservative lithogenic elements (Ti, Zr, Al, and Rb) to study anthropogenic element enrichments in lake sediments. J. Paleolimnol. 46, 75–87. https://doi.org/10.1007/s10933-011-9515-z.

Bossard, M., Feranec, J., Otahel, J., 2000. CORINE land cover technical guide – Addendum 2000. European Environmental Agency ETC/LC, Copenhagen.

Büntgen, U., Tegel, W., Nicolussi, K., McCormick, M., Frank, D., Trouet, V., Kaplan, J.O., Herzig, F., Heussner, K.-U., Wanner, H., Luterbacher, J., Esper, J., 2011. 2500 Years of European Climate Variability and Human Susceptibility. Science (80-.) 331, 578–582. https://doi.org/10.1126/science.1197175.

Charreau, J., Blard, P.-H., Puchol, N., Avouac, J.-P., Lallier-Vergès, E., Bourlès, D., Braucher, R., Gallaud, A., Finkel, R., Jolivet, M., Chen, Y., Roy, P., 2011. Paleo-erosion rates in Central Asia since 9Ma: A transient increase at the onset of Quaternary glaciations? Earth Planet. Sci. Lett. 304, 85–92. https://doi.org/10.1016/j.epsl.2011.01.018.

Chassiot, L., Miras, Y., Chapron, E., Develle, A., Arnaud, F., Motelica-heino, M., Di Giovanni, C., 2018. A 7000-year environmental history and soil erosion record inferred from the deep sediments of Lake Pavin (Massif Central, France). Palaeogeogr. Palaeoclimatol. Palaeoecol. 497, 2018–2233. https://doi.org/10.1016/j.palaeo.2018.02.024.

Cross, J.A., 2001. Megacities and small towns: different perspectives on hazard vulnerability. Glob. Environ. Chang. Part B Environ. Hazards 3, 63–80. https://doi.org/10.3763/ehaz.2001.0307.

Davies, S.J., Lamb, H.F., Roberts, S.J., 2015. In: Micro-XRF Core Scanning in Palaeolimnology: Recent Developments BT – Micro-XRF Studies of Sediment Cores: Applications of a non-destructive tool for the environmental sciences. Springer, Netherlands, Dordrecht, pp. 189–226. https://doi.org/10.1007/978-94-017-9849-5_7.

De Ploey, J., Moeyersons, J., Goossens, D., 1995. The De Ploey erosional susceptibility model for catchments, ES. CATENA 25, 269–314. https://doi.org/10.1016/0341-8162(95)00014-J.

De Roo, A., Schmuck, G., Perdigao, V., Thielen, J., 2003. The influence of historic land use changes and future planned land use scenarios on floods in the Oder catchment. Phys. Chem. Earth, Parts A/B/C 28, 1291–1300. https://doi.org/10.1016/j.pce.2003.09.005.

De Vos, W., Tarvainen, T., Salminen, R., Reeder, S., De Vivo, B., Demetriades, A., Pirc, S., Batista, M., Marsina, K., Ottesen, R., O'connor, P., 2006. Geochemical Atlas of Europe: Part 2: Interpretation of geochemical maps, additional tables, figures, maps, and related publications. Geological Survey of Finland, Espoo, Finland.

Di-Giovanni, C., Disnar, J.R., Bichet, V., Campy, M., Guillet, B., 1998. Geochemical characterization of soil organic matter and variability of a postglacial detrital organic supply (chaillexon lake, france). Earth Surf. Process. Landforms 23, 1057–1069. https://doi.org/10.1002/(SICI)1096-9837(199812)23:12<1057::AID-ESP921>3.0.CO;2-H.

Doyen, E., Bégeot, C., Simonneau, A., Millet, L., Chapron, E., Arnaud, F., Vannière, B., 2016. Land use development and environmental responses since the Neolithic around Lake Paladru in the French Pre-alps. J. Archaeol. Sci. Reports 7, 48–59. https://doi.org/10.1016/j.jasrep.2016.03.040.

Feranec, J., Hazeu, G., Christensen, S., Jaffrain, G., 2007. Corine land cover change detection in Europe (case studies of the Netherlands and Slovakia). Land use policy 24, 234–247. https://doi.org/10.1016/j.landusepol.2006.02.002.

Foucher, A., Salvador-Blanes, S., Evrard, O., Simonneau, A., Chapron, E., Courp, T., Cerdan, O., Lefèvre, I., Adriaensen, H., Lecompte, F., Desmet, M., 2014. Increase in soil erosion after agricultural intensification: Evidence from a lowland basin in France. Anthropocene 7, 30–41. https://doi.org/10.1016/j.ancene.2015.02.001.

Garcia-Pausas, J., Casals, P., Camarero, L., Huguet, C., Sebastià, M.T., Thompson, R., Romanyà, J., 2007. Soil organic carbon storage in mountain grasslands of the Pyrenees: effects of climate and topography. Biogeochemistry 82, 279–289. https://doi.org/10.1007/s10533-007-9071-9.

Gascoin, S., Fanise, P., 2018. "Bernadouze meteorological data". 10.6096/DV/UQITZ4, SEDOO OMP, V2.

Graz, Y., Di-Giovanni, C., Copard, Y., Laggoun-Défarge, F., Boussafir, M., Lallier-Vergès, E., Baillif, P., Perdereau, L., Simonneau, A., 2010. Quantitative palynofacies analysis as a new tool to study transfers of fossil organic matter in recent terrestrial environments. Int. J. Coal Geol. 84, 49–62. https://doi.org/10.1016/j.coal.2010.08.006.

Guillemot, T., Bichet, V., Simonneau, A., Rius, D., Massa, C., Gauthier, E., Richard, H., Magny, M., 2015. Impact of Holocene climate variability on lacustrine records and human settlements in South Greenland. Clim. Past 11, 5401–5438. https://doi.org/10.5194/cpd-11-5401-2015.

Holzhauser, H., Magny, M., Zumbuühl, H.J., 2005. Glacier and lake-level variations in west-central Europe over the last 3500 years. The Holocene 15, 789–801. https://doi.org/10.1191/0959683605hl853ra.

Hosek, J., Pokorný, P., Prach, J., Lenka, L., Grygar, M., Knésl, I., Truba, J., 2017. Late Glacial erosion and pedogenesis dynamics : Evidence from high-resolution lacustrine archives and paleosols in south Bohemia (Czech Republic). Catena 150, 261–278. https://doi.org/10.1016/j.catena.2016.11.022.

Hyland, E., Sheldon, N., Van der Voo, R., Badgley, C., Abrajevitch, A., 2015. A New paleoprecipitation proxy based on soil magnetic properties: implications for expanding paleoclimate reconstructions. Geol. Soc. Am. Bull. https://doi.org/10.1130/B31207.1.

Jin, Z., Wang, S., Shen, J., Zhang, E., Li, F., Ji, J., Lu, X., 2001. Chemical weathering since the Little Ice Age recorded in lake sediments: a high-resolution proxy of past climate. Earch Surf. Process. Landforms 26, 775–782. https://doi.org/10.1002/esp.224.

Lana-Renault, N., Regüés, D., Martí-Bono, C., Beguería, S., Latron, J., Nadal, E., Serrano, P., García-Ruiz, J.M., 2007. Temporal variability in the relationships between precipitation, discharge and suspended sediment concentration in a small Mediterranean mountain catchment. Hydrol. Res. 38, 139–150. https://doi.org/10.2166/nh.2007.003.

Liu, Y., Gupta, H.V., 2007. Uncertainty in hydrologic modeling : Toward an integrated data assimilation framework. Water Resour. Res. 43, 1–18. https://doi.org/10.1029/2006WR005756.

Magny, M., Vannière, B., Calo, C., Millet, L., Leroux, A., Peyron, O., Zanchetta, G., La Mantia, T., Tinner, W., 2011. Holocene hydrological changes in south-western Mediterranean as recorded by lake-level fluctuations at Lago Preola, a coastal lake in southern Sicily. Italy. Quat. Sci. Rev. 30, 2459–2475. https://doi.org/10.1016/j.quascirev.2011.05.018.

Maher, B.A., Thompson, R., 1995. Paleorainfall reconstructions from pedogenic magnetic susceptibility variations in the chinese loess and paleosols. Quat. Res. 44, 383–391. https://doi.org/10.1006/qres.1995.1083.

Marquer, L., Mazier, F., Sugita, S., Galop, D., Houet, T., van Beek, P., Faure, E., Gaillard, M., Haunold, S., de Munnik, N., Simonneau, A., de Vleeschouwer, F., Le Roux, G., 2019. Pollen-based reconstruction of Holocene land-cover in mountain regions: evaluation of the Landscape Reconstruction Algorithm in the Vicdessos valley (Northern Pyrenees, France). Quat. Sci. Rev.

Melquiades, F.L., Appoloni, C.R., 2004. Application of XRF and field portable XRF for environmental analysis. J. Radioanal. Nucl. Chem. 262, 533–541. https://doi.org/10.1023/B:JRNC.0000046792.52385.b2.

Meteo France, 2019. Données publiques – Données SYNOP essentielles OMM [WWW Document]. Meteo Fr. URL https://donneespubliques.meteofrance.fr/?fond=produit&id_produit=90&id_rubrique=32 (accessed 4.4.19).

Mügler, I., Gleixner, G., Günther, F., Mäusbacher, R., Daut, G., Schütt, B., Berking, J., Schwalb, A., Schwark, L., Xu, B., Yao, T., Zhu, L., Yi, C., 2010. A multi-proxy approach to reconstruct hydrological changes and Holocene climate development of Nam Co, Central Tibet. J. Paleolimnol. 43, 625–648. https://doi.org/10.1007/s10933-009-9357-0.

Noël, H., Garbolino, E., Brauer, A., Lallier-Vergès, E., de Beaulieu, J.-L., Disnar, J.-R., 2001. Human impact and soil erosion during the last 5000 yrs as recorded in lacustrine sedimentary organic matter at Lac d'Annecy, the French Alps. J. Paleolimnol. 25, 229–244. https://doi.org/10.1023/A:1008134517923.

Oliva, P., Dupré, B., Martin, F., Viers, J., 2004. The role of trace minerals in chemical weathering in a high-elevation granitic watershed (Estibère, France): Chemical and mineralogical evidence. Geochim. Cosmochim. Acta 68, 2223–2244. https://doi.org/10.1016/j.gca.2003.10.043.

Ouahabi, M., Hubert-Ferrari, A., Fagel, N., 2016. Lacustrine clay mineral assemblages as a proxy for land-use and climate changes over the last 4 kyr: The Amik Lake case study. Southern Turkey. Quat. Int. https://doi.org/10.1016/j.quaint.2016.11.032.

Pawełczyk, F., Chróst, L., Magiera, T., Michczyński, A., Sikorski, J., Tudyka, K., Zajac, E., 2017. Radiocarbon and Lead-210 age-depth model and trace elements concentration in the wolbrom fen (S Poland). Geochronometria 44, 40–48. https://doi.org/10.1515/geochr.

Peyron, O., Guiot, J., Cheddadi, R., Tarasov, P., Reille, M., de Beaulieu, J.-L., Bottema, S., Andrieu, V., 1998. Climatic Reconstruction in Europe for 18,000 YR B.P. from Pollen Data. Quat. Res. 49, 183–196. https://doi.org/10.1006/qres.1997.1961.

Quintana-Seguí, P., Turco, M., Herrera, S., Miguez-Macho, G., 2017. Validation of a new SAFRAN-based gridded precipitation product for Spain and comparisons to Spain02 and ERA-Interim. Hydrol. Earth Syst. Sci. 21, 2187–2201. https://doi.org/10.5194/hess-21-2187-2017.

Renard, K., Freimund, J., 1994. Using monthly precipitation data to estimate the R-factor in the revised USLE. J. Hydrol. 157, 287–306. https://doi.org/10.1016/0022-1694(94)90110-4.

Ritchie, J.C., McHenry, J.R., 1990. Application of Radioactive Fallout Cesium-137 for measuring soil erosion and sediment accumulation rates and patterns: a review. J.

Environ. Qual. 19, 215–233. https://doi.org/10.2134/jeq1990.00472425001900020006x.

Rosenmeier, M.F., Hodell, D.A., Brenner, M., Curtis, J.H., Martin, J.B., Anselmetti, F.S., Ariztegui, D., Guilderson, T.P., 2002. Influence of vegetation change on watershed hydrology: implications for paleoclimatic interpretation of lacustrine δ18O records. J. Paleolimnol. 27, 117–131. https://doi.org/10.1023/A:1013535930777.

Rozanski, K., Johnsen, S.J., Schotterer, U., Thompson, L.G., 1997. Reconstruction of past climates from stable isotope records of palaeo-precipitation preserved in continental archives. Hydrol. Sci. J. 42, 725–745. https://doi.org/10.1080/02626669709492069.

Sabatier, P., Poulenard, J., Fanget, B., Reyss, J., Develle, A., Wilhelm, B., Ployon, E., Pignol, C., Naffrechoux, E., Dorioz, J., Montuelle, B., Arnaud, F., 2014. Long-term relationships among pesticide applications, mobility, and soil erosion in a vineyard watershed. PNAS 111, 15647–15652. https://doi.org/10.1073/pnas.1411512111.

Salminen, R., Batista, M., Bidovec, M., Demetriades, A., De Vivo, B., De Vos, W., Duris, M., Gilucis, A., Gregorauskiene, V., Halamić, J., Heitzmann, P., Lima, A., Jordan, G., Klaver, G., Klein, P., Lis, J., Locutura, J., Marsina, K., Mazreku, A., O'Connor, P., Olsson, S., Ottesen, R.-T., Petersell, V., Plant, J., Reeder, S., Salpeteur, I., Sandstrom, H., Siewers, U., Steenfelt, A., Tarvainen, T., 2015. Geochemical atlas of Europe, part 1, background information, methodology and maps. Geological survey of Finland.

Schmidt, R., Kamenik, C., Tessadri, R., Koinig, K., 2006. Climatic changes from 12,000 to 4,000 years ago in the Austrian Central Alps tracked by sedimentological and biological proxies of a lake sediment core. J. Paleolimnol. 35, 491–505. https://doi.org/10.1007/s10933-005-2351-2.

Seddon, A.W.R., Mackay, A.W., Baker, A.G., Birks, H.J.B., Breman, E., Buck, C.E., Ellis, E.C., Froyd, C.A., Gill, J.L., Gillson, L., Johnson, E.A., Jones, V.J., Juggins, S., Macias-Fauria, M., Mills, K., Morris, J.L., Nogués-Bravo, D., Punyasena, S.W., Roland, T.P., Tanentzap, A.J., Willis, K.J., Aberhan, M., van Asperen, E.N., Austin, W.E.N., Battarbee, R.W., Bhagwat, S., Belanger, C.L., Bennett, K.D., Birks, H.H., Bronk Ramsey, C., Brooks, S.J., de Bruyn, M., Butler, P.G., Chambers, F.M., Clarke, S.J., Davies, A.L., Dearing, J.A., Ezard, T.H.G., Feurdean, A., Flower, R.J., Gell, P., Hausmann, S., Hogan, E.J., Hopkins, M.J., Jeffers, E.S., Korhola, A.A., Marchant, R., Kiefer, T., Lamentowicz, M., Larocque-Tobler, I., López-Merino, L., Liow, L.H., McGowan, S., Miller, J.H., Montoya, E., Morton, O., Nogué, S., Onoufriou, C., Boush, L.P., Rodriguez-Sanchez, F., Rose, N.L., Sayer, C.D., Shaw, H.E., Payne, R., Simpson, G., Sohar, K., Whitehouse, N.J., Williams, J.W., Witkowski, A., 2014. Looking forward through the past: identification of 50 priority research questions in palaeoecology. J. Ecol. 102, 256–267. https://doi.org/10.1111/1365-2745.12195.

Sikorski, J., 2019. A new method for constructing Pb-210 chronology of young peat profiles sampled with low frequency. Geochronometria 46, 1–14. https://doi.org/10.1515/geochr-2015-0101.

Simonneau, A., 2012. Empreintes climatiques et anthropiques sur le détritisme holoc'ene : 'etude multiparam'etres et intégrée de syst'emes lacustres d'Europe Occidentale. Université d'Orléans.

Simonneau, A., Chapron, E., Courp, T., Tachikawa, K., Le Roux, G., Baron, S., Galop, D., Garcia, M., Di Giovanni, C., Motellica-heino, M., Mazier, F., Foucher, A., Houet, T., Desmet, M., Bard, E., 2013. Recent climatic and anthropogenic imprints on lacustrine systems in the Pyrenean Mountains inferred from minerogenic and organic clastic supply (Vicdessos valley, Pyrenees, France). The Holocene1–14. https://doi.org/10.1177/0959683613505340.

Simonneau, A., Chapron, E., Garçon, M., Winiarski, T., Graz, Y., Chauvel, C., Debret, M., Motelica-heino, M., Desmet, M., Di Giovanni, C., 2014. Tracking Holocene glacial and high-altitude alpine environments fl uctuations from minerogenic and organic markers in proglacial lake sediments (Lake Blanc Huez, Western French Alps). Quat. Sci. Rev. 89, 27–43. https://doi.org/10.1016/j.quascirev.2014.02.008.

Simonneau, A., Chapron, E., Vanniere, B., Wirth, S.B., Gilli, A., Di-giovanni, C., Anselmetti, F.S., Desmet, M., Magny, M., 2013. Mass-movement and flood-induced deposits in Lake Ledro, southern Alps, Italy : implications for Holocene palaeohydrology and natural hazards. Clim. Past 9, 825–840. https://doi.org/10.5194/cp-9-825-2013.

Simonneau, A., Doyen, E., Chapron, E., Millet, L., Vannière, B., Di Giovanni, C., Bossard, N., Tachikawa, K., Bard, E., Albéric, P., Desmet, M., Roux, G., Lajeunesse, P., Berger, J.F., Arnaud, F., 2013. Holocene land-use evolution and associated soil erosion in the French Prealps inferred from Lake Paladru sediments and archaeological evidences. J. Archaeol. Sci. 40, 1636–1645. https://doi.org/10.1016/j.jas.2012.12.002.

Sugita, S., 2007. Theory of quantitative reconstruction of vegetation II: All you need is LOVE. Holocene 17, 243–257. https://doi.org/10.1177/0959683607075838.

Summer, W., Walling, D., 2002. Modelling erosion, sediment transport and sediment yield. Paris.

Vidal, J.P., Martin, E., Franchistéguy, L., Baillon, M., Soubeyroux, J.M., 2010. A 50-year high-resolution atmospheric reanalysis over France with the Safran system. Int. J. Climatol. 30, 1627–1644. https://doi.org/10.1002/joc.2003.

Wang, G., Gertner, G., Singh, V., Shinkareva, S., Parysow, P., Anderson, A., 2002. Spatial and temporal prediction and uncertainty of soil loss using the revised universal soil loss equation: a case study of the rainfall – runoff erosivity R factor. Ecol. Modell. 153, 143–155. https://doi.org/10.1016/s0304-3800(01)00507-5.

Wang, H., Liu, L., Feng, Z., 2008. Spatiotemporal variations of Zr/Rb ratio in three last interglacial paleosol profiles across the Chinese Loess Plateau and its implications for climatic interpretation. Chinese Sci. Bull. 53, 1413–1422. https://doi.org/10.1007/s11434-008-0068-0.

Wilhelm, B., Arnaud, F., Sabatier, P., Crouzet, C., Chaumillon, E., Disnar, J., Guiter, F., Reyss, J., Wilhelm, B., Arnaud, F., Sabatier, P., Crouzet, C., Brisset, E., 2012. 1400 years of extreme precipitation patterns over the Mediterranean French Alps and pos-

sible forcing mechanisms. Quat. Res. 78, 1–12. https://doi.org/10.1016/j.yqres.2012.03.003>.

Wischnewski, J., Mischke, S., Wang, Y., Herzschuh, U., 2011. Reconstructing climate variability on the northeastern Tibetan Plateau since the last Lateglacial – a multi-proxy, dual-site approach comparing terrestrial and aquatic signals. Quat. Sci. Rev. 30, 82–97. https://doi.org/10.1016/j.quascirev.2010.10.001.

Zhou, W., Xian, F., Du, Y., Kong, X., Wu, Z., 2014. The last 130ka precipitation reconstruction from Chinese loess 10Be. J. Geophys. Res. Solid Earth 119, 191–197. https://doi.org/10.1002/2013JB010296.Received.

Ziadat, F.M., Taimeh, A.Y., 2013. Effect of rainfall intensity, slope, land use and antecedent soil moisture on soil erosion in an arid environment. L. Degrad. Dev. 24, 582–590. https://doi.org/10.1002/ldr.2239.